Georgia Southern University

From the SelectedWorks of Eric Loren Johnson

2014

The Ã 2Δ5/2-X 2Δ5/2 Electronic Band System of Nickel Acetylide, NiCCH

Eric L. Johnson, *Georgia Southern University*
Michael Morse

Available at: https://works.bepress.com/eric-loren-johnson/2/

Molecular Physics, 2015
Vol. 113, Nos. 15–16, 2255–2266, http://dx.doi.org/10.1080/00268976.2015.1023751

Taylor & Francis
Taylor & Francis Group

Downloaded by [University of Utah] at 12:10 13 September 2015

INVITED ARTICLE

The $\tilde{A}^2\Delta_{5/2} \leftarrow \tilde{X}^2\Delta_{5/2}$ electronic band system of nickel acetylide, NiCCH

Eric L. Johnson and Michael D. Morse*

Department of Chemistry, University of Utah, Salt Lake City, UT, USA

(*Received 26 November 2014; accepted 22 February 2015*)

Optical spectra of the supersonically cooled NiCCH radical have been recorded in the 530–650 nm region using the resonant two-photon ionisation method, and five of the observed bands have been rotationally resolved. The rotationally resolved studies demonstrate that the ground state of NiCCH is of $\tilde{X}^2\Delta_{5/2}$ symmetry, corresponding to a $3d^9$ configuration on the nickel atom, with the hole located in a $3d\delta$ orbital. Most of the observed bands are assigned to the $\tilde{A}^2\Delta_{5/2} \leftarrow \tilde{X}^2\Delta_{5/2}$ electronic transition, which shows a progression in the Ni–C stretching mode, ν_3. In addition, single excitations of the modes ν_2 (C≡C stretch), ν_4 (C≡C–H bend), and ν_5 (Ni–C≡C bend) are observed, allowing these vibrational intervals to be determined for the $\tilde{A}^2\Delta_{5/2}$ state. Hot bands also allow the determination of ν_5 in the ground $\tilde{X}^2\Delta_{5/2}$ state. Quantum chemical computations have also been performed, confirming that the ground state is of $^2\Delta$ symmetry. The results are placed in context via comparison to other monovalent, monoligated Ni complexes, particularly NiCu, NiH, and NiCN.

Keywords: electronic spectrum; electronic structure; NiCCH radical; laser spectroscopy

1. Introduction

Nickel and organonickel compounds are critically important as catalytic reagents in modern synthetic organic chemistry [1]. Probably, the first example of the use of an organonickel reagent is the Mond process, which was developed in the 1890s and uses volatile nickel tetracarbonyl to purify nickel from impure nickel powder [2]. Another early example of the use of nickel in organic chemistry is Raney nickel, a powdered nickel–aluminium alloy that was developed in 1926 as a catalyst for the hydrogenation of vegetable oil [3]. More recently, nickel has been employed as a more cost-efficient replacement for palladium in the Heck reaction for the benzylation or arylation of alkenes [4–6]. These examples truly just scratch the surface of the uses of nickel in catalytic chemistry. Other examples include the Reppe synthesis of cyclooctatetraene [7], the Kumada coupling of organic halides with Grignard reagents [8,9], and the Negishi cross-coupling reaction [10]. Nickel acetylides, especially those with the $Ni(C{\equiv}CR)_2L_2$ structure, are useful as catalysts in organic chemistry [11], particularly in the polymerisation of methyl methacrylate [12–14] and of alkynes [15,16]. In these catalysts, nickel is typically either zerovalent (Raney nickel and $Ni(CO)_4$) or divalent (as in $Ni(C{\equiv}CR)_2L_2$). Nevertheless, in order to obtain an improved understanding of the nickel–acetylide bond, we have undertaken a study of the electronic spectroscopy of NiCCH, where nickel is monovalent (Ni^+). This work complements and extends our previous studies of the transition metal acetylides CuCCH [17] and CrCCH [18,19].

Prior to this work, neutralisation–reionisation mass spectrometric studies had proved that neutral NiCCH is physically stable as a chemically bound molecule with a lifetime greater than 1 μs [20]. Further, fragmentation patterns from the collision-induced dissociation measurements strongly suggested a linear NiCCH structure, rather than a vinylidene structure [20]. This result is confirmed in the present investigation.

Regardless of whether one considers the molecule to be ionic, as Ni^+ CCH^-, or covalent, as Ni–C≡C–H, the singly ligated nickel atom may be considered to have a valence of one and to have an open $3d^9$ subshell. Thus, NiCCH joins a long list of monoligated, monovalent nickel molecules that have been spectroscopically investigated by this group and others [21–69]. In order of increasing electronegativity of the ligand (provided on the Allred–Pauling [70] scale in parentheses), these previously studied species include NiAl (1.61) [21,22], NiCu (1.90) [23–26], NiH (2.20) [27–33], NiAu (2.54) [22,34], NiI (2.66) [35–39], NiBr (2.96) [40–43], NiCl (3.16) [43–52], and NiF (3.98) [53–67]. In addition to these diatomic species, NiCN has also been investigated [68,69]. Nickel acetylide is expected to be similar to NiCN, as the group electronegativities of CN and CCH are similar, although the precise values of this quantity depend on the procedure employed in its estimation. Both ligands are also similar in having empty π^* orbitals that are available to receive nickel $d\pi$ electron density. In a recent computation and critical evaluation of group electronegativities, the electronegativities of CCH and CN are listed as 3.11 and 3.19 on the Pauling scale, respectively, placing

*Corresponding author. Email: morse@chem.utah.edu

© 2015 Taylor & Francis

NiCCH and NiCN on either side of NiCl in the ordered list above [71].

The hole in the nickel $3d^9$ subshell in these molecules can be located in the $3d\sigma$, $3d\pi$, or $3d\delta$ orbital, leading to $^2\Sigma^+$, $^2\Pi$, or $^2\Delta$ states. The spin–orbit interaction then causes the $^2\Pi$ and $^2\Delta$ states to split into $^2\Pi_{1/2}$, $^2\Pi_{3/2}$, $^2\Delta_{3/2}$, and $^2\Delta_{5/2}$ levels, and spin–orbit mixing between the $^2\Sigma^+$ and $^2\Pi_{1/2}$ states and between the $^2\Pi_{3/2}$ and $^2\Delta_{3/2}$ states causes the Λ value to become ill-defined in these states. It is only in the $^2\Delta_{5/2}$ state that Λ is expected to remain a good quantum number. Previous experiments have shown that the ground state for the systems with relatively electropositive ligands (NiAl through NiI, and NiCN) have $^2\Delta_{5/2}$ ground states, while the more electronegative ligands cause NiBr, NiCl, and NiF to have ground states of mixed $^2\Pi$ and $^2\Delta$ character, with $\Omega = 3/2$. Theoretical investigations of the splitting of the $3d^9$ core in the field of a ligand have been provided by several research groups [32,72–74].

Section 2 describes the experimental methods used to investigate NiCCH, while Section 3 presents computational and experimental results. These are discussed and compared to related molecules in Section 4, and the most important conclusions from this work are summarised in Section 5.

2. Experimental

In the current work, nickel acetylide, NiCCH, was investigated using resonant two-photon ionisation spectroscopy (R2PI). The instrument employed is identical to that used in previous studies [17–19,75–77]. Molecular NiCCH is produced by focusing the third harmonic radiation from a Q-switched Nd:YAG laser (355 nm) onto a 1:1 nickel–gold sample at a point that is 1.3 cm upstream from the expansion orifice of a pulsed supersonic expansion of helium (40–60 psig backing pressure) that is seeded with 0.0025% acetylene. The NiAu sample was used in previous experiments [22,34], and was convenient for the present study; there is no reason why a pure nickel sample would not have worked equally well. The sample is rotated and translated to prevent holes from being drilled; this provides a relatively constant signal intensity. The products of the laser ablation process are entrained in the carrier gas and travel through a 1.3-cm-long reaction zone prior to expansion through a 2-mm orifice into vacuum. The supersonic expansion into the vacuum chamber cools the ablation products to a rotational temperature of approximately 6 K. The molecular beam is then roughly collimated by a 1 cm diameter skimmer and enters the Wiley-McLaren ion source of a reflectron time-of-flight mass spectrometer [78,79]. In the ion source, the molecular beam is exposed to tuneable dye laser radiation that is counterpropagated along the beam path. Following a delay of about 20 ns, the molecules are exposed to the output radiation of an F_2 excimer laser (157 nm, 7.87 eV) that intersects the molecular beam at right angles. Any ions produced are accelerated in a static electric field into a time-of-flight tube, and are reflected down a second flight tube to a dual microchannel plate detector. The ion signal is preamplified, digitised, and the ion signals of interest are stored for subsequent analysis on a personal computer. The entire experiment is repeated at a rate of 10 Hz.

Low-resolution spectra of ^{58}NiCCH (mass 83 Da) and ^{60}NiCCH (mass 85 Da) were recorded from 15,400 to 18,800 cm^{-1}. To reveal the rotational structure of the observed bands, high-resolution scans were performed by inserting an air-spaced etalon into the oscillator cavity of the dye laser, which was then pressure scanned using SF_6. Calibration of the rotationally resolved bands was accomplished using two partial reflections of the dye laser light. One was directed through a cell containing gaseous I_2, and the transmission spectrum was recorded using a photodiode detector. The other was directed to a 0.22 cm^{-1} free spectral range etalon, and the transmission fringes were recorded. The spectra obtained were linearised using the transmission fringes and then calibrated using the I_2 atlas of Gerstenkorn and Luc [80,81]. Corrections were made to account for the error in the I_2 atlas, -0.0056 cm^{-1} [81], and for the Doppler shift experienced by the molecules as they approach the radiation source at the beam velocity of helium, 1.77×10^5 cm/s [82]. Combined, the two corrections amount to about 0.10 cm^{-1} for the bands examined here.

Along with high-resolution spectra, excited-state lifetimes were also collected for selected bands by firing the ionisation laser at the time of peak NiCCH signal intensity, while the dye laser was scanned in time as the NiCCH$^+$ ion signal was monitored. The resulting decay curves measure the number of NiCCH molecules that remain in states that are readily ionised as a function of time. The measured curves were fitted to an exponential decay model using the Levenberg–Marquardt non-linear least-squares algorithm [83]. Three independent lifetime curves were collected and fitted for each band; the standard deviation of the three values is reported as the 1σ error limit.

3. Results

3.1. Computations on NiCCH

To aid in the assignment of the spectra, density functional theory (DFT) calculations employing the B3LYP hybrid density functional method in combination with the aug-cc-pVTC Dunning correlation consistent basis set [84] were undertaken for the $^2\Sigma^+$, $^2\Pi$, and $^2\Delta$ states of NiCCH that arise from the $3d^9$ occupation on nickel. These were performed using the Gaussian 09W suite of programs [85]. At this level of theory, the $^2\Delta$ state was found to be the ground state. The $^2\Sigma^+$ and $^2\Pi$ states are calculated to lie 384 and 1282 cm^{-1} above the $^2\Delta$ state, respectively. Calculated energies, bond lengths, vibrational frequencies, and dipole moments of the three low-lying states are provided

Downloaded by [University of Utah] at 12:10 13 September 2015

Table 1. Computed and measured results on ^{58}NiCCH.[a]

Property	$^2\Delta$	$^2\Sigma^+$	$^2\Pi$	$\tilde{X}\,^2\Delta$ (exp)	$\tilde{A}\,^2\Delta$ (exp)
Energy[b]	0	383.86	1282.45	0	15,940.041(561)
r(Ni–C)[c]	1.8312	1.8502	1.8550		
r(C≡C)[c]	1.2121	1.2133	1.2139		
r(C–H)[c]	1.0625	1.0624	1.0628		
$\nu_1(\sigma^+$, C–H stretch)[b]	3451.09	3451.18	3447.37		
$\nu_2(\sigma^+$, C≡C stretch)[b]	2080.58	2071.66	2053.08		2001.9(1.4)
$\nu_3(\sigma^+$, Ni–C stretch)[b]	496.94	476.63	474.17		458.4(1.0)
$\nu_4(\pi$, C≡C–H bend)[b]	675.02	667.63	652.30		636.5(0.9)
			712.56		
$\nu_5(\pi$, Ni–C≡C bend)[b]	225.04	207.99	208.72	209.5(0.6)	221.2(2.2)
			222.22		
Dipole moment (D)	3.474	3.910	3.454		

[a]As described in the text, all computations were done using the Gaussian 09W suite of programs. The molecule was found to be linear in all calculations, although the different frequencies for the bending modes in the $^2\Pi$ term indicate that a Renner–Teller effect is expected. See text for details.
[b]Given in cm^{-1} units.
[c]Given in Å units.

Downloaded by [University of Utah] at 12:10 13 September 2015

in Table 1. The vibrational frequencies deduced from the spectra that are described later are also provided for comparison.

When a group of states is as closely spaced as these three states, spin–orbit interaction can be important in determining the absolute ordering of the states. If we treat the partially occupied orbitals as having pure Ni 3d character, it is straightforward to approximate the effects of spin–orbit interaction using the spin–orbit Hamiltonian matrices provided by Spain and Morse [72]. For the $^2\Delta_{5/2}$ level, which undergoes no spin–orbit coupling with the other states, the energy is given by

$$E(^2\Delta_{5/2}) = T(^2\Delta) - \zeta_{3d}\,(\mathrm{Ni})\,, \tag{3.1}$$

where $T(^2\Delta)$ is the term energy of the $^2\Delta$ state, as obtained from the computational results, and ζ_{3d}(Ni) is the atomic spin–orbit parameter for the 3d orbitals of nickel, which is tabulated as 670 cm^{-1} [86]. For the remaining levels, states with the same value of Ω are mixed by the spin–orbit interaction, leading to Hamiltonian matrices that must be diagonalised to obtain the final predicted energy levels. These matrices are

$$\begin{pmatrix} T(^2\Pi) - \frac{\zeta_{3d}(\mathrm{Ni})}{2} & -\zeta_{3d}\,(\mathrm{Ni}) \\ -\zeta_{3d}\,(\mathrm{Ni}) & T(^2\Delta) + \zeta_{3d}\,(\mathrm{Ni}) \end{pmatrix} \text{for } \Omega = \frac{3}{2} \text{ levels} \tag{3.2}$$

and

$$\begin{pmatrix} T(^2\Sigma^+) & -\sqrt{\frac{3}{2}}\,\zeta_{3d}\,(\mathrm{Ni}) \\ -\sqrt{\frac{3}{2}}\,\zeta_{3d}\,(\mathrm{Ni}) & T(^2\Pi) + \frac{\zeta_{3d}(\mathrm{Ni})}{2} \end{pmatrix} \text{for } \Omega = \frac{1}{2} \text{levels.} \tag{3.3}$$

Using the term energies obtained from the B3LYP calculations, in combination with the value ζ_{3d}(Ni) = 670 cm^{-1}, we obtain a final predicted set of low-lying states in NiCCH as given in Table 2. These bear a striking similarity to the known low-lying states in the closely related NiCN molecule, also listed in Table 2. The close correspondence between the calculated levels of NiCCH and the measured levels of NiCN shows that the two molecules are electronically very similar.

From the point of view of analysing the spectra obtained in this study, the vibrational frequencies calculated in NiCCH are particularly important. As was found in our

Table 2. Calculated spin–orbit levels of the 3d^9 states of NiCCH, compared to measured states of NiCN.

Calculated states of NiCCH			Measured states of NiCN[a]	
Ω	Energy (cm^{-1})	Composition	Designation	Energy (cm^{-1})
5/2	0	100% $^2\Delta_{5/2}$	$^2\Delta_{5/2}$	0
1/2	644	80% $^2\Sigma^+$; 20% $^2\Pi_{1/2}$		
3/2	795	60% $^2\Delta_{3/2}$; 40% $^2\Pi_{3/2}$	$^2\Delta_{3/2}$	830
3/2	2163	60% $^2\Pi_{3/2}$; 40% $^2\Delta_{3/2}$	$^2\Pi_{3/2}$	2238
1/2	2697	80% $^2\Pi_{1/2}$; 20% $^2\Sigma^+$		

[a]From Reference [68].

studies of CuCCH [17] and CrCCH [18], the calculated vibrational frequencies are well-separated and are expected to be readily distinguished in the spectra. This is very helpful for making vibronic assignments.

3.2. *Vibronic spectrum*

The vibronically resolved spectrum of ^{58}NiCCH is displayed in Figure 1, and the locations of the observed bands are listed in Table 3. The spectrum is dominated by one electronic band system, designated as the $\tilde{A} \leftarrow \tilde{X}$ system, although a few additional features are observed. The most intense feature in the spectrum, near 15,910 cm^{-1}, is assigned as the 0_0^0 band based on isotopic shift measurements (see below). A series of bands spaced by roughly 450 cm^{-1} extends toward higher wave numbers. Based on the correspondence between these values, the computed results for the Ni–CCH stretching mode, and the excited-state frequencies of the Cr–CCH (425.6 cm^{-1}) [18] and Cu–CCH (479, 466.8, and 462 cm^{-1}) [17] stretching modes, the progression is assigned to mode ν_3, the Ni–CCH stretch. A corresponding series of weaker features, shifted to lower wave numbers by 209.5 cm^{-1}, is assigned as hot bands arising from ground-state molecules in which the Ni–C≡C bending mode (ν_5) is singly excited. Because this mode carries one unit of vibrational angular momentum, transitions to levels lacking vibrational angular momentum (as is the

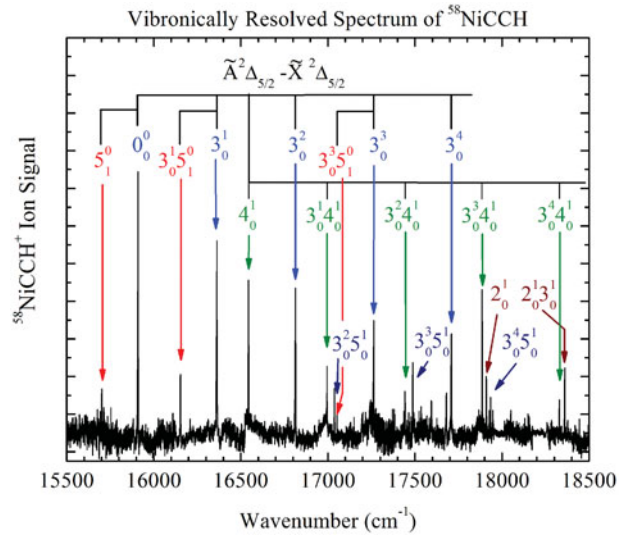

Figure 1. Vibronically resolved spectrum of ^{58}NiCCH, showing the $\tilde{A}^2\Delta_{5/2} \leftarrow \tilde{X}^2\Delta_{5/2}$ band system.

Table 3. Bands measured for ^{58}NiCCH.

Band	Measured ν_0 (cm^{-1})	Fitted ν_0 (cm^{-1})	Residual in fit (cm^{-1})	Isotope shift ν(^{58}NiCCH)-ν(^{60}NiCCH) (cm^{-1})	B' (cm^{-1})	P'	τ (μs)
$\tilde{A} - \tilde{X}\ 5_1^0$	15,701.2[b]	15,701.531	0.669[d]				
$\tilde{A} - \tilde{X}\ 0_0^0$	15,910.1[b]	15,910.041	0.059[d]	0.1			0.725(15)[c]
$\tilde{A} - \tilde{X}\ 3_0^1 5_1^0$	16,153.6[b]	16,153.795	−0.195[d]	1.7			0.739(74)[c]
$\tilde{A} - \tilde{X}\ 3_0^1$	16,362.8830(27)[c]	16,363.305	−0.422[d]	1.96	0.12931(10)[c]	5/2	0.802(18)[c]
$\tilde{A} - \tilde{X}\ 4_0^1$	16,544.1[b]	16,544.817	−0.717[d]				
$\tilde{A} - \tilde{X}\ 3_0^2$	16,813.8[b]	16,814.152	−0.352[d]	3.8			0.820(47)[c]
$\tilde{A} - \tilde{X}\ 3_0^1 4_0^1$	16,994.7834(27)[c]	16,994.578	0.205[d]	1.8	0.12878(11)[c]	7/2	1.243(29)[c]
$\tilde{A} - \tilde{X}\ 3_0^2 5_0^1$	17,037.7539(30)[c]	17,037.709	0.045[d]	1.9	0.12893(8)[c]	7/2	1.456(63)[c]
$\tilde{A} - \tilde{X}\ 3_0^3 5_1^0$	17,052.6[b]	17,053.074	−0.474[d]				
$\tilde{A} - \tilde{X}\ 3_0^3$	17,262.7[b]	17,262.584	0.116[d]	5.9			
U[a]	17,437.2[b]						
$\tilde{A} - \tilde{X}\ 3_0^2 4_0^1$	17,443.4[b]	17,441.923	1.477[d]	3.9			
$\tilde{A} - \tilde{X}\ 3_0^3 5_0^1$	17,487.0[b]	17,487.090	−0.090[d]	4.0			1.74(19)[c]
U[a]	17,594.2704(68)[c]				0.12820(14)[c]	5/2	7.98(1.08)[c]
U[a]	17,680.3[b]			7.1			18.7(1.2)[c]
$\tilde{A} - \tilde{X}\ 3_0^4$	17,709.2[b]	17,708.601	0.599[d]	7.1			
$\tilde{A} - \tilde{X}\ 3_0^3 4_0^1$	17,886.1530(90)[c]	17,886.852	−0.699[d]	5.9	0.12869(14)[c]	7/2	
$\tilde{A}\ 2_0^1$	17,910.5[b]	17,910.500	0.000[d]	−0.1			
U[a]	17,927.1[b]						
$\tilde{A} - \tilde{X}\ 3_0^4 5_0^1$	17,934.1[b]	17,934.055	0.045[d]				
U[a]	17,946.1[b]						
$\tilde{A} - \tilde{X}\ 3_0^4 4_0^1$	18,329.1[b]	18,329.365	−0.265[d]	7.5			
$\tilde{A} - \tilde{X}\ 2_0^1 3_0^1$	18,360.9[b]	18,360.900	0.000[d]	2.0			

[a]Unidentified band.
[b]Estimated band–origin location, measured in low-resolution, expected accuracy ± 1 cm^{-1}.
[c]Error limits (1σ) are provided in parentheses, in units of the last digits quoted.
[d]Residual is defined as measured value minus fitted value. The least-squares fit of the measured vibronic levels to Equation (3.6) provides the values listed in Table 4.

Downloaded by [University of Utah] at 12:10 13 September 2015

Downloaded by [University of Utah] at 12:10 13 September 2015

case here) have vanishing Franck–Condon factors. Thus, these bands have a different source of oscillator strength than the main progression, gaining intensity by vibronic coupling with another state.

It proved more difficult than expected to measure accurate isotope shifts between the more abundant isotopologue, ^{58}NiCCH (83 Da, 66.75%), and the less abundant one, ^{60}NiCCH (85 Da, 25.53%), because of large fluctuating background signals at the mass of ^{60}NiCCH. These large fluctuating signals also appeared at a significantly reduced intensity in mass 87 Da, leading us to suspect that they may be due to AlNi molecules, for which the abundant species have masses of 85 Da (68.3% abundance) and 87 Da (26.1% abundance). This molecule has an ionisation energy of 6.95 ± 0.09 eV [21], making it readily one photon ionised by the F_2 excimer laser (7.89 eV); therefore, even small amounts of AlNi produced via Al impurities can easily overwhelm the signal due to ^{60}NiCCH. The fact that these features became much more intense when we polished the sample with Al_2O_3 sandpaper reinforces this assignment. Apart from the rotationally resolved work on the $\tilde{A} - \tilde{X}\ 3_0^1$ band, all of isotope shift measurements were obtained from low-resolution scans conducted prior to polishing the sample.

To verify the vibrational assignment, the molecule was treated as a pseudo-diatomic, and the isotope shift was modelled by fitting the progression in the ν_3 mode for the ^{58}NiCCH isotopologue to the diatomic formula,

$$\nu_{v'-0} = T_0 + v'\omega_e' - (v'^2 + v')\omega_e' x_e'. \tag{3.4}$$

The fitted molecular constants ω_e' and $\omega_e' x_e'$ could then be used to calculate the predicted isotope shift using the following formula [87]:

$$\begin{aligned}\nu\left(^{58}\text{NiCCH}\right) - \nu\left(^{60}\text{NiCCH}\right) &= (\rho - 1)\left[\omega_e'\left(v' + 1/2\right) - \omega_e''(1/2)\right] \\ &\quad - \left(\rho^2 - 1\right)\left[\omega'_e x_e'\left(v' + 1/2\right)^2 - \omega_e'' x_e''(1/2)^2\right],\end{aligned} \tag{3.5}$$

where the dimensionless parameter, ρ, is given as $\rho = \sqrt{\frac{\mu(^{60}\text{Ni-CCH})}{\mu(^{58}\text{Ni-CCH})}} = 1.00506$. By treating Equations (3.4) and (3.5) as functions of a continuous parameter, v', it was possible to plot the predicted isotope shift, $\nu(^{58}\text{NiCCH}) - \nu(^{60}\text{NiCCH})$, as a function of the band frequency, $\nu_{v'-0}$, for various assignments of the bands. The resulting curves were then compared to the measured isotope shifts to identify the correct vibrational numbering. To do so, the ground-state vibrational frequency, ω_e'', was taken as 497 cm^{-1} from the DFT calculations using the B3LYP/cc-pVTZ basis set, and the anharmonicity, $\omega_e'' x_e''$, was neglected. The result, displayed in Figure 2, shows clearly that the 15,910 cm^{-1} band is the 0_0^0 band. This assignment gives a pseudo-diatomic vibrational frequency of 454.6 ± 0.4 cm^{-1} and an anharmonicity of 0.98 ± 0.07 cm^{-1} in the excited electronic state.

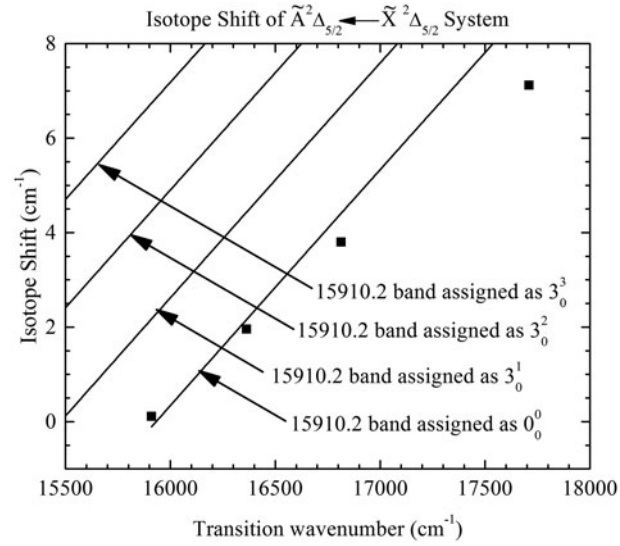

Figure 2. Isotope shift of the bands of the $\tilde{A}^2\Delta_{5/2} \leftarrow \tilde{X}^2\Delta_{5/2}$ band system, demonstrating that the 15,910 cm^{-1} band is the 0_0^0 band of this system.

A weaker series of bands, occurring at 16,544.1, 16,994.8, 17,443.4, 17,886.2, and 18,329.1 cm^{-1}, also forms a progression with a pseudo-diatomic vibrational frequency of 453.8 ± 1.3 cm^{-1} and an anharmonicity of 1.5 ± 0.3 cm^{-1}. A plot of the measured isotope shifts is displayed in Figure 3, confirming that the first of these bands, at 16,544.1 cm^{-1}, has no quanta of the Ni–CCH vibrational

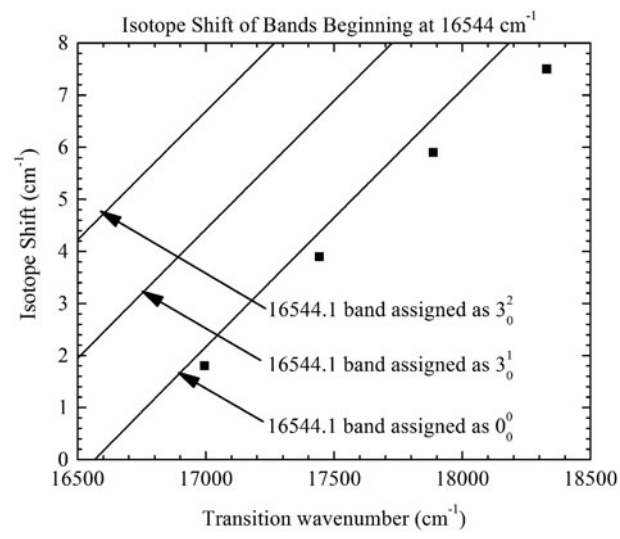

Figure 3. Isotope shift of the weak bands beginning at 16,544.1 cm^{-1}. This plot demonstrates that these bands form a progression, and that the 16,544.1 cm^{-1} band has no quanta excited in the Ni–CCH stretching mode, ν_3.

Downloaded by [University of Utah] at 12:10 13 September 2015

mode excited. Although it is possible that these features could correspond to a different excited state of NiCCH, the similarity between the vibrational frequency of this progression (453.8 cm^{-1}) and that of the $\tilde{A}$ state (454.6 cm^{-1}) strongly suggests that the new progression also corresponds to a set of vibrational levels in the $\tilde{A}$ state. The first band in this progression is found to be 634.0 cm^{-1} to the blue of the $\tilde{A} - \tilde{X}$ 0_0^0 band, which is in reasonably good agreement with the calculated frequencies of the C≡C–H bending mode, ν_4. Accordingly, we assign these features to the 4_0^1, $3_0^1 4_0^1$, $3_0^2 4_0^1$, $3_0^3 4_0^1$, and $3_0^4 4_0^1$ bands of the $\tilde{A} - \tilde{X}$ system.

As demonstrated in rotationally resolved studies later, the main progression of 3_0^n bands are $\Omega' = 5/2 \leftarrow \Omega'' = 5/2$ parallel transitions, while these $3_0^n 4_0^1$ features have one unit of vibrational angular momentum in the upper state due to the excitation of the π-symmetry ν_4 mode, making them perpendicular transitions. Defining the quantum number P as the combined electronic and vibrational angular momentum around the axis, given by $P \equiv \Lambda + \ell + \Sigma = \Omega + \ell$, the $3_0^n 4_0^1$ features are $P' = 7/2 \leftarrow P'' = \Omega'' = 5/2$ transitions. The other expected set of vibronic levels arising from the coupling of the ν_4 bending mode ($\ell = \pm 1$) to the electronic angular momentum of $\Omega' = 5/2$, giving an upper state $P' = 3/2$, is not observed. This implies that the $3_0^n 4_0^1$ progression gains intensity through vibronic coupling with an electronic state with $\Omega' = 7/2$, but that vibronic coupling to states with $\Omega' = 3/2$ is much weaker, preventing the observation of the $P' = 3/2$ set of vibronic levels.

Another vibrational progression is evident in the data in the weak bands at 17,037.8, 17,487.0, and 17,934.1 cm^{-1}. Fitting these features as the 0_0^0, 3_0^1, and 3_0^2 bands of a new band system yields a pseudo-diatomic vibrational frequency and anharmonicity of 451.4 cm^{-1} and 1.07 cm^{-1}, again quite close to that found for the $\tilde{A} - \tilde{X}$ system. Rotational resolution of the weak feature at 17,037.8 cm^{-1} shows that this transition has a symmetry of $P' = 7/2 \leftarrow P'' = \Omega'' = 5/2$. Again, these features could arise from a totally different excited state, but the close similarity in the pseudo-diatomic vibrational frequency is evidence that this progression also belongs to the $\tilde{A} - \tilde{X}$ system. These three bands are found 224.5 ± 0.6 cm^{-1} to the blue of the 3_0^2, 3_0^3, and 3_0^4 bands, respectively, consistent with an assignment as combination bands involving one unit of the Ni–C≡C π-bending mode, ν_5. This assignment shows a slight stiffening of the Ni–C≡C bending mode upon electronic excitation, from a frequency of $\nu_5'' = 209.5$ cm^{-1} to $\nu_5' = 224.5$ cm^{-1}, which is not unreasonable. As a comparison, excitation of CuCCH from the $\tilde{X}^1\Sigma^+$ ground state to the $\tilde{A}^1\Sigma^+$ and $\tilde{B}\ ^1\Pi$ states increased the frequency of the ν_5 Cu–C≡C bending mode from 242.9 cm^{-1} to 284.4 and 267 cm^{-1}, respectively [17]. Therefore, these bands are assigned as the $3_0^2 5_0^1$, $3_0^3 5_0^1$, and $3_0^4 5_0^1$ bands of the $\tilde{A} - \tilde{X}$ system. Again, the combination of one unit of vibrational angular momentum ($\ell = \pm 1$) from ν_5' with the upper state $\Omega' = 5/2$ can lead to either $P' = 3/2$ or $P' = 7/2$, but the bands with $P' = 7/2$ show significantly greater oscillator strength, and are observed. The bands with $P' = 3/2$ are presumably too weak to observe in our experiments. This is again presumably due to vibronic coupling with an excited electronic state with $\Omega' = 7/2$.

Two features are found at 17,910.5 and 18,360.9 cm^{-1} with isotope shifts of −0.1 and 2.0 cm^{-1}, respectively. These are consistent with transitions in which mode 3, the Ni–C stretching mode, has no excitation and one unit of excitation, respectively. These could correspond to the 0_0^0 and 3_0^1 bands of a completely different band system, but their separation, 450.4 cm^{-1}, is again close to that found for other ν_3 excitations in the $\tilde{A}$ state. These bands are separated from 0_0^0 and 3_0^1 bands by 2000.4 and 1998.0 cm^{-1}, respectively. These intervals are close to what might be expected for excitation of ν_2, the C≡C stretch. Because of the close match between the 450.4 cm^{-1} interval found here and the other ν_3 intervals found in the spectrum, we assign these features to the 2_0^1 and $2_0^1 3_0^1$ bands of the $\tilde{A} - \tilde{X}$ system.

In addition to these 18 bands that are assigned to the $\tilde{A} - \tilde{X}$ system, 5 additional bands were observed that could not be classified into this system. These are also listed in Table 3. These weak features likely correspond to excitations to other electronic states that have lower oscillator strength. A large number of excited electronic states are expected for NiCCH in this region, arising from the $3d^8 4s^1$, ^2F, and ^4F states of Ni^+ interacting with CCH^-. Although one of these bands was rotationally resolved, we have little additional information about these features. They were generally too weak to warrant further study at this time.

The vibronic bands that are assigned to the $\tilde{A}^2\Delta_{5/2} - \tilde{X}^2\Delta_{5/2}$ system were fitted to the anharmonic energy expression,

$$\begin{aligned} \nu = T_0 &- \omega_5'' v_5'' + \omega_2' v_2' + \omega_3' v_3' + \omega_4' v_4' + \omega_5' v_5' \\ &+ x_{33}' \left(v_3'^2 + v_3'\right) + x_{23}' \left(v_2' v_3' + \frac{v_2' + v_3'}{2}\right) \\ &+ x_{34}' \left(v_3' v_4' + \frac{v_3' + v_4'}{2}\right) + x_{35}' \left(v_3' v_5' + \frac{v_3' + v_5'}{2}\right). \end{aligned} \tag{3.6}$$

The fitted wave numbers and residuals in the fit are given in Table 3. The resulting molecular constants are provided, along with their 1σ error limits, in Table 4.

3.3. *Rotationally resolved spectra of NiCCH*

A rotationally resolved scan over the 3_0^1 band of the $\tilde{A} \leftarrow \tilde{X}$ system is displayed in Figure 4, along with a negative-going simulation of the spectrum, computed using the PGopher program [88], in blue. The band shows obvious R, Q, and P branches, with a band head in the R branch, indicating that the rotational constant decreases upon electronic excitation, corresponding to a lengthening of the Ni–C

Table 4. Fitted vibrational constants for the $\tilde{A}^2\Delta_{5/2} \leftarrow \tilde{X}^2\Delta_{5/2}$ system of NiCCH.

Constant	Value (cm^{-1})	Constant	Value (cm^{-1})
ν_0	15,940.041 ± 0.561	ω_5'	221.184 ± 2.299
ω_5''	209.510 ± 0.576	x_{33}'	−1.208 ± 0.132
ω_2'	2001.891 ± 1.405	x_{23}'	−2.864 ± 1.160
ω_3'	458.388 ± 1.019	x_{34}'	−3.503 ± 0.316
ω_4'	636.528 ± 0.928	x_{35}'	0.949 ± 0.651

bond. In addition, the large gap between the first R and P lines indicates large Ω values in both the upper and lower states. Analysis of the spectrum shows that it arises from an $\Omega' = 5/2 \leftarrow \Omega'' = 5/2$ transition, with first lines of R(2.5), Q(2.5), and P(3.5). Given that the only state with $\Omega'' = 5/2$ that arises from the d^9 configuration is the $^2\Delta_{5/2}$ state, this spectrum proves that the ground state is of $^2\Delta_{5/2}$ symmetry. As should be expected, the ground state of NiCCH is electronically analogous to that of the isoelectronic molecule, NiCN [68,69]. This is also consistent with the B3LYP/aug-cc-pVTZ calculations.

The decay lifetime of the $\tilde{A}$ state, measured for various vibronic levels, varies in the range from 0.72 to 1.8 μs. In a polyatomic molecule such as NiCCH, the decay process could include non-radiative decay mechanisms in addition to fluorescence. However, under the collision-free conditions of the experiment, non-radiative decay mechanisms would produce a vibrationally hot NiCCH molecule in a lower electronic state; the total energy would be conserved. It is possible that the molecule would remain ionisable using the F_2 laser, but with reduced efficiency. This could lead to a bi-exponential decay curve, with the initial depopulation of the pumped state showing a rapid decay, followed by a slower decay as the non-radiatively populated state decays further. When all of the excitation energy is degraded into vibrational motion on the ground electronic state, poor Franck–Condon factors would likely prevent efficient ionisation, giving only background signal levels. For aromatic organic molecules with rapid singlet to triplet intersystem crossing, followed by a slower triplet to ground-state singlet intersystem crossing process, this process has been observed. The time-delayed resonant two-photon ionisation method has been used to measure the vibrationally excited triplet-state lifetime as a function of vibrational energy content [89,90].

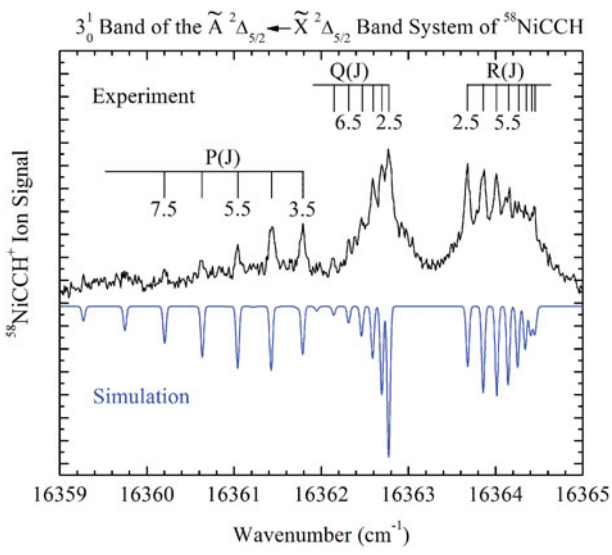

Figure 4. Rotationally resolved scan over the 3_0^1 band of the $\tilde{A}^2\Delta_{5/2} \leftarrow \tilde{X}^2\Delta_{5/2}$ band system. The first lines prove that both upper and lower states have $\Omega = 5/2$.

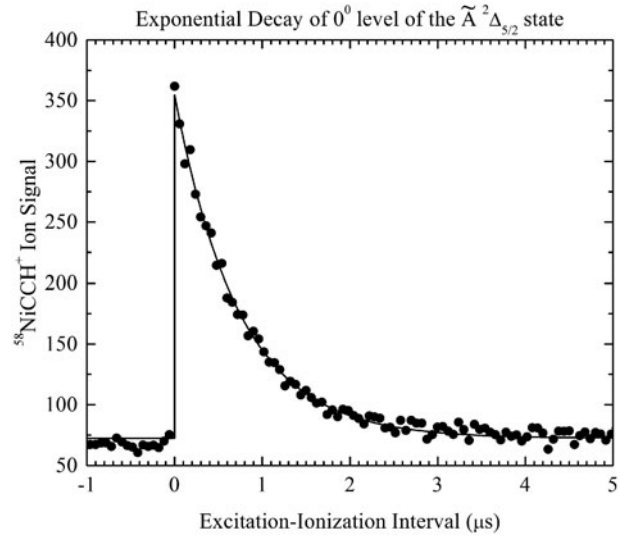

Figure 5. Exponential decay of the 0^0 level of the $\tilde{A}^2\Delta_{5/2}$ state, measured by the time-delayed resonant two-photon ionisation method. The fit of this decay curve gives $\tau = 0.730$ μs; combined with two other measurements, a value of $\tau = 0.725 \pm 0.015$ μs is obtained.

We believe that the measured excited-state lifetimes found for NiCCH are true fluorescence lifetimes, without complications due to non-radiative decay. An example of the measured lifetime and the quality of the fit is given in Figure 5, which displays no evidence of bi-exponential behaviour. In addition, the measured lifetimes (0.72–1.8 μs, depending on vibronic level; 8.0 μs for a level that belongs to a different electronic state) are comparable to those found for diatomic nickel species, where the density of states is certainly inadequate for radiationless decay under collision-free conditions. Examples include molecules whose lifetimes have been measured in the ranges 3.6 to over 40 μs (NiCu, with the longest lifetime corresponding to quartet states) [23,24], 6–10 μs (NiAu) [34], 0.17–10 μs (NiSi) [91], and 0.07–0.6 μs (NiC) [92], respectively. It should be noted that the transitions in these diatomic nickel species (and in NiCCH) are primarily 3d ← 3d or 4s ← 3d excitations that are forbidden in the atom, but become allowed through mixing with 4p orbitals in the molecules.

Downloaded by [University of Utah] at 12:10 13 September 2015

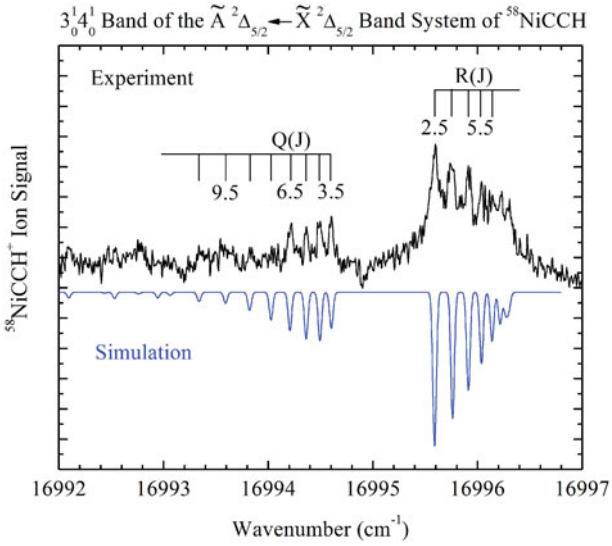

Figure 6. Rotationally resolved scan over the $3^1_0 4^1_0$ band of the $\tilde{A}^2\Delta_{5/2} \leftarrow \tilde{X}^2\Delta_{5/2}$ band system. The intense R branch is evidence that $\Delta\Omega = 1$ in this band, and the first lines of R(2.5) and Q(3.5) prove that $\Omega'' = 5/2$, $P' = 7/2$.

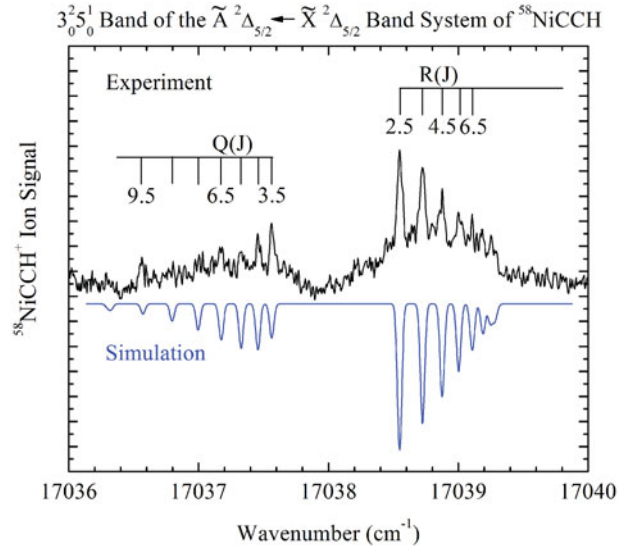

Figure 7. Rotationally resolved scan over the $3^2_0 5^1_0$ band of the $\tilde{A}^2\Delta_{5/2} \leftarrow \tilde{X}^2\Delta_{5/2}$ band system. The intense R branch is evidence that $\Delta\Omega = 1$ in this band, and the first lines of R(2.5) and Q(3.5) prove that $\Omega'' = 5/2$, $P' = 7/2$.

As a result, fully allowed excitations in these molecules tend to have lifetimes on the order of 500 ns to 2 μs. Because the 4p orbitals lie significantly above the 3d or 4s orbital, there is a strong correlation of fluorescence lifetime with the excitation energy of the band system, with higher energy excited states generally having significantly shorter lifetimes. This is due to the greater contribution of 4p character in the higher energy states, along with the shortening of the lifetimes by the ν^3 factor that appears in the Einstein A coefficient.

Given that the low-lying electronic states are all doublets arising from the $3d^9$ configuration on the nickel core, the ~1 μs fluorescence lifetime establishes that the upper state is primarily doublet in character. Doublet states that have $\Omega' = 5/2$ are $^2\Delta_{5/2}$ and $^2\Phi_{5/2}$, but a $^2\Phi_{5/2} \leftarrow \tilde{X}\,^2\Delta_{5/2}$ transition is forbidden by the $\Delta\Sigma = 0$ selection rule. Therefore, the upper state is assigned as a $^2\Delta_{5/2}$ state. The band system is assigned as the $\tilde{A}\,^2\Delta_{5/2} \leftarrow \tilde{X}\,^2\Delta_{5/2}$ system.

Figure 6 displays the rotationally resolved scan over the $3^1_0 4^1_0$ band near 16,695 cm^{-1}. The intense R branch shows that the quantum number P increases in this excitation, and the first lines demonstrate that $P' = 7/2$, $P'' = \Omega'' = 5/2$. The upper state P' value includes the vibrational angular momentum of the ν_4 C≡C–H bending mode and provides strong evidence that the band has been properly assigned as having one excitation of a bending mode. A rotationally resolved scan over the $3^3_0 4^1_0$ band near 17,886 cm^{-1} displays the same intensity pattern and first lines, as expected; therefore, it is not reproduced here. The scan, along with a simulated spectrum, is available in the Supplementary Material for this article.

Figure 7 displays a scan over the $3^2_0 5^1_0$ band near 17,038 cm^{-1}, which is similar in appearance to the $3^1_0 4^1_0$ band shown in Figure 6. Again, the band is clearly a $P' = 7/2 \leftarrow \Omega'' = 5/2$ band, confirming that a bending mode has been excited in this transition. In this case, it is the low-frequency Ni–C≡C ν_5 mode that is excited in combination with two quanta of the Ni–C stretching vibration.

The remaining band that was rotationally resolved is a band near 17,594 cm^{-1} that has a much longer fluorescence lifetime ($\tau = 7.98 \pm 1.08$ μs) and appears to belong to a different band system. It is an $\Omega' = 5/2 \leftarrow \Omega'' = 5/2$ band that probably gains oscillator strength through mixing between its upper state and the $\tilde{A}^2\Delta_{5/2}$ state investigated here. Assuming that the upper state arises from the $d^8(^3F)s^1$, $^{2,4}F$ configuration of Ni^+, as is known in the examples of NiCu and NiH, this state could be of $^2\Phi_{5/2}$, $^4\Phi_{5/2}$, $^4\Delta_{5/2}$, or $^4\Pi_{5/2}$ symmetry [72]. In NiCu [72], NiH [72], and NiCN [68], the $^2\Phi_{5/2}$ state lies 1645, 2446, and 2520 cm^{-1} above the $\tilde{A}^2\Delta_{5/2}$ state, respectively. The unknown band in NiCCH lies 1684 cm^{-1} above the $\tilde{A}^2\Delta_{5/2}$ state, which is a bit low in energy, if we consider NiCCH to be electronically similar to NiCN. An alternative possibility is a state dominated by $^4\Phi_{5/2}$ character, which lies lower than the equivalent of the $\tilde{A}^2\Delta_{5/2}$ state of NiCu and NiH by 383 and 464 cm^{-1}, respectively [72]. If this is the case, it is likely that the unknown band corresponds to a vibrationally excited level of the $^4\Phi_{5/2}$ state. Further speculation is not warranted at this time. The rotationally resolved spectrum of the 17,594 cm^{-1} band, along with a simulated spectrum and measured and fitted line positions, is provided in the Supplementary Material for this article.

Downloaded by [University of Utah] at 12:10 13 September 2015

Table 5. Fitted molecular constants of resolved bands of ^{58}NiCCH.[a]

Band	$\tilde{A}-\tilde{X}\ 3_0^1$	$\tilde{A}-\tilde{X}\ 3_0^1 4_0^1$	$\tilde{A}-\tilde{X}\ 3_0^2 5_0^1$	[17.59]5/2 - $\tilde{A}\ 0_0$	$\tilde{A}-\tilde{X}\ 3_0^3 4_0^1$
T_0	16,362.8830(27)	16,994.7834(27)	17,037.7539(30)	17,594.2704(68)	17,886.1530(90)
B'	0.12931(10)	0.12878(11)	0.12893(8)	0.12820(14)	0.12869(14)
P'	5/2	7/2	7/2	5/2	7/2
B''	0.14080(11)	0.14080(11)	0.14080(11)	0.14080(11)	0.14080(11)
Ω''	5/2	5/2	5/2	5/2	5/2

[a]All values are in cm^{-1} units. Error limits in the fitted molecular constants (1σ) are provided in parentheses after each constant, in units of the last digit quoted. In the fit, all of the bands were constrained to have the same value of B''.

All of the rotationally resolved bands originate from a lower level with $\Omega'' = 5/2$ and are found to have very similar rotational constants. Therefore, it seems clear that they arise from the same vibronic level. Although, in principle, this might be a metastable state that remains populated in the molecular beam, the only example in which we have found a metastable state of a nickel-containing molecule is in Ni_2 [93,94]. In our experiments on NiCu [23,24], NiAu [34], AlNi [21], NiC [92], NiSi [91], NiPd [95], and NiPt [96], we have found only one electronic state to be populated. Thus, we assign the ground state as the $\tilde{X}^2\Delta_{5/2}$ state, deriving from a d^9 configuration on the nickel atom.

Accordingly, all rotationally resolved bands were constrained to have the same lower state rotational constant in a combined fit, allowing a more precise value of this quantity to be determined. In the fit, all of the bands were fitted to the Hund's case (a) or (c) formula [87]:

$$\nu = \nu_0 + B'J'\left(J'+1\right) - B''J''\left(J''+1\right). \qquad (3.7)$$

The resulting molecular constants are provided in Table 5. The line positions are provided in the supplementary information. The fitted value of B'' obtained for ^{58}NiCCH is 0.14080(11) cm^{-1}. Here, as elsewhere in this report, the value in parentheses represents the 1σ error limit, in units of the last digits quoted.

4. Discussion

As in all of the known monovalent, monoligated nickel molecules, the ground state of NiCCH derives from a 3d^9 configuration on nickel. Like NiAl [21,22], NiCu [23–26], NiH [27–33], NiAu [22,34], NiI [35–39], and NiCN [68,69], NiCCH preferentially places the 3d hole in the 3dδ orbital, leading to an $\tilde{X}\ ^2\Delta_{5/2}$ ground state. This differs from the ground state when more electronegative ligands are present, which has $\Omega = 3/2$ for NiCl [43–52] and NiF [53–67].

If we consider the 3d orbitals of Ni^+ to be too contracted to bond significantly with the orbitals of the ligand, and instead consider the 3d orbital splitting to be governed by electrostatic interactions, it is only possible to obtain a $^2\Delta$ ground term by assigning the ligand a positive effective charge. A negative ligand charge would cause the 3dσ orbital, which points toward the ligand, to be destabilised, causing the Ni 3d orbitals to fall in the order of increasing energy as 3dδ < 3dπ < 3dσ. This favours placement of the 3d hole in the 3dσ orbital, leading to a term ordering of $^2\Sigma^+ < {}^2\Pi < {}^2\Delta$, in contradiction to the experiment, which shows a $^2\Delta_{5/2}$ ground state. Although a positive ligand charge is counterintuitive, reasonably good fits to the calculated [72] or measured [26] electronic levels of the 3d^9 configuration of NiCu are obtained when a ligand charge of $Z_{Cu} = +1$ is employed. A positive ligand charge would also be required to account for the energy ordering of the 3d^9 states in NiH, which follows the same pattern found in NiCu. This result may be rationalised by recognising that in these molecules, which are more covalent than ionic, the σ bonding electrons lie in a relatively diffuse orbital with substantial $4s_{Ni}$ character. To whatever extent that the σ^2 electrons occupy a diffuse, nearly spherical orbital around the Ni atom, they are not effective in splitting the 3dσ, 3dπ, and 3dδ orbitals. Instead, it is the underlying +1 ion core on the ligand that favours placement of the hole in the 3dδ orbital.

In NiH [32,72], NiCN [68], and NiCu [72], the manifold of excited states in the 10,000–20,000 cm^{-1} range arises from the 3d^{8}4s^1, ^{2}F, and ^{4}F states of the Ni^+ ion, combined with an H^-, CN^-, or Cu^- anion. The known electronic states of all three molecules show identical energy orderings, to the extent that they are experimentally known, as displayed in Figure 8. For this group of states, the energy levels in NiCu and NiH can be well fitted by a ligand field model in which the ligand carries a negative charge of −0.666 for NiCu and −0.439 for NiH [72]. In both NiCu and NiH, the pattern of 3d^{8}4s^1 states is mainly governed by the exchange interaction between the 4s^1 electron and the 3d^8 core, and by the spin–orbit interaction within the 3d^8 core [72]. These effects are expected to be largely independent of the ligand, although the exchange effects can be reduced if the ligand is able to delocalise the 4s^1 electron significantly. To the extent that the CN^- anion acts as a non-interacting negatively charged ligand, a similar pattern of states would be expected. Figure 8 shows that this is apparently the case, with the NiCN excited states closely

Downloaded by [University of Utah] at 12:10 13 September 2015

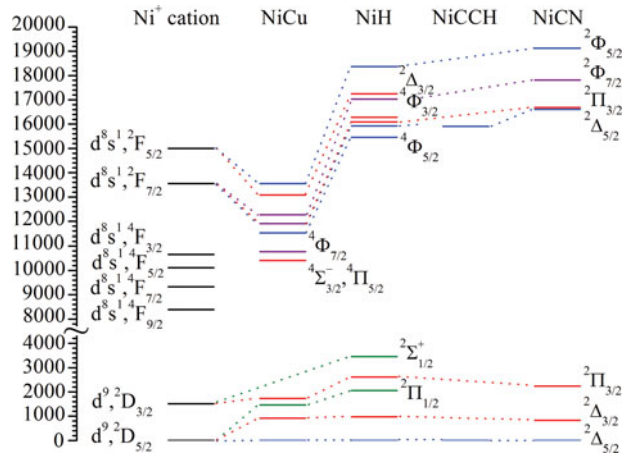

Figure 8. Experimentally known electronic states of Ni^+, NiCu, NiH, NiCCH, and NiCN. In this figure, states with $\Omega = 0.5$ are displayed using green horizontal lines, while states with $\Omega = 3/2$ are indicated in red. States with $\Omega = 5/2$ are indicated with blue horizontal lines, and states with $\Omega = 7/2$ are indicated by purple. Although many of the states are strongly mixed by spin–orbit interaction, the dominant Hund's case (a) term is listed above. Labels that are provided next to the NiCN column correlate all the way across the table, as shown. Labels provided next to the NiH column correlate in some cases to NiCu, as shown by the dotted correlation lines. The $^4\Phi_{7/2}$ and the nearly degenerate $^4\Pi_{5/2}$ and $^4\Sigma^-_{3/2}$ states are only known in NiCu and are found in the 10,000–11,000 cm^{-1} region.

following the NiH pattern of states, as was originally observed by Kingston *et al*. [68]. Given that we have only identified one of the expected $3d^84s^1$ excited states in the NiCCH molecule, we are unable to prove that it will also follow the same pattern, but we see no reason to expect otherwise.

The NiCCH molecule is isoelectronic with NiCN, differing only by the replacement of the nitrogen atom with a CH group. Thus, the two molecules are not merely isoelectronic; they differ only in the replacement of a triply bonded N atom by a triply bonded CH group. This allows the vibrational motions of the two species to be usefully compared. The Ni–C≡N bending mode in the $\tilde{X}\ ^2\Delta_{5/2}$ ground state exhibits a first excited level that is 243.4 cm^{-1} above the ground level [68], while in NiCCH, the ground-state Ni–C≡C bending interval is somewhat reduced from this value, 209.5 cm^{-1}. One might expect the two molecules to have quite similar Ni–C stretching frequencies, but we unfortunately have not measured this quantity for the ground state. The $\tilde{A}\ ^2\Delta_{5/2}$ state of NiCN differs from that of NiCCH, however, in that the vibrational intervals corresponding to excitation of the Ni–CN stretch exhibit a negative anharmonicity, with intervals ranging from 433 to 450 cm^{-1}. This probably results from perturbations by the nearby $\tilde{B}\ ^2\Pi_{3/2}$ state, which lies only 79 cm^{-1} above the $\tilde{A}\ ^2\Delta_{5/2}$ state. In contrast, the Ni–CCH stretching progression observed in the $\tilde{A}^2\Delta_{5/2} \leftarrow \tilde{X}^2\Delta_{5/2}$ band system is quite regular, with intervals in the 3^n_0 progression dropping smoothly from 452.8 to 446.5 cm^{-1} as one moves from the 0^0_0 band to the 3^4_0 band. Likewise, in the $\tilde{A}^2\Delta_{5/2}$state of NiCN, the Ni–C≡N bending mode is strongly anharmonic, with the first excited level lying 180.2 cm^{-1} above the ground level. This compares to a value of 224 cm^{-1} in the case of NiCCH. These results show that the vibrational frequencies of the two molecules are quite similar, overall.

It is worth noting that the ν_2' excited state C≡C vibrational frequency is now known for two transition metal monoacetylides, NiCCH and CrCCH. In these species, the ground state corresponds to a d^9 Ni^+ ion and a d^5 Cr^+ ion, respectively, interacting with a C_2H^- anion. In the excited states, these metal ions are excited to d^8s^1 and d^4s^1 configurations, respectively. The C≡C vibrational frequency in the $\tilde{A}^2\Delta_{5/2}$ and $\tilde{A}^6\Sigma^+$ states of NiCCH and CrCCH are 2001.9 cm^{-1} and 1944.3 cm^{-1} [18], respectively. The large decrease in the excited state C≡C vibrational frequency in moving from NiCCH to CrCCH is consistent with a model in which there is a more significant transfer of metal dπ electron density into the C≡C π anti-bonding orbital in the case of CrCCH as compared to NiCCH, leading to a more significant weakening of the C≡C bond. This would be favoured by the more electropositive nature of Cr compared to Ni, and by the larger size and greater accessibility of the 3d orbitals of Cr as compared to Ni. It would be interesting to see if this trend is followed in the other transition metal acetylides, both in the excited state and in the ground state.

5. Conclusions

The first spectroscopic investigation of NiCCH has been performed using the resonant two-photon ionisation method. The molecule has been shown to be linear, with a ground state of $\tilde{X}^2\Delta_{5/2}$ symmetry. The electronic transition to the $\tilde{A}^2\Delta_{5/2}$ state has been extensively studied, allowing the rotational constants of both the upper and lower states to be measured, and permitting vibrational levels associated with excitations in the ν_2, ν_3, ν_4, and ν_5 modes in the upper state to be identified. The Ni–C≡C bending frequency in the ground state has also been measured through the observation of hot bands. The $\tilde{A}^2\Delta_{5/2}$–$\tilde{X}^2\Delta_{5/2}$ excitation is found to lie quite close to the corresponding excitation in NiCN, and the vibrational frequencies of NiCCH are found to be similar to the analogous vibrational frequencies of NiCN. Further, it is suggested that the overall pattern of electronic states deriving from the $3d^9$ and $3d^84s^1$ manifolds will be quite similar to that found in NiCN and NiH.

Acknowledgements

This paper is dedicated to John P. Maier in appreciation of his body of superb spectroscopic work. The authors thank Prof. Peter B. Armentrout for very helpful assistance in the computational work.

Downloaded by [University of Utah] at 12:10 13 September 2015

Downloaded by [University of Utah] at 12:10 13 September 2015

Disclosure statement

No potential conflict of interest was reported by the authors.

Funding

This work was funded by the Division of Chemical Sciences, Geosciences, and Biosciences, Office of Basic Energy Sciences of the US Department of Energy [grant number DE-FG02-01ER15176].

Supplemental data

Supplemental data for this article can be accessed at http://dx.doi.org/10.1080/00268976.2015.1023751.

References

[1] T.-Y. Luh and L.-F. Huang, Handb. Funct. Organomet. **2**, 397 (2005).
[2] L. Mond, C. Langer, and F. Quincke, J. Chem. Soc. Trans. **57**, 749 (1890).
[3] T.-K. Yang, D.-S. Lee, and J. Haas, *e-EROS Encyclopedia of Reagents for Organic Synthesis*, (2006). <http://onlinelibrary.wiley.com/doi/10.1002/047084289X.rr001.pub2/full>.
[4] R. Matsubara, A.C. Gutierrez, and T.F. Jamison, J. Am. Chem. Soc. **133**, 19020 (2011).
[5] T.M. Goegsig, J. Kleimark, S.O. Nilsson Lill, S. Korsager, A.T. Lindhardt, P.-O. Norrby, and T. Skrydstrup, J. Am. Chem. Soc. **134**, 443 (2012).
[6] Z. Tasker Sarah, C. Gutierrez Alicia, and F. Jamison Timothy, Angew. Chem. Int. Ed. **53**, 1858 (2014).
[7] J.-C. Hsieh and C.-H. Cheng, Chem. Commun. (**19**), 2459 (2005).
[8] R.J.P. Corriu and J.P. Masse, J. Chem. Soc. Chem. Commun. (**3**), 144 (1972).
[9] K. Tamao, K. Sumitani, and M. Kumada, J. Am. Chem. Soc. **94**, 4374 (1972).
[10] A.O. King, N. Okukado, and E. Negishi, J. Chem. Soc. Chem. Commun. (**19**), 683 (1977).
[11] G.G. Melikyan and K.M. Nicholas, Mod. Acetylene Chem. 99 (1995). <doi:10.1002/9783527615278.ch04>.
[12] H. Sun, Q. Shen, X. Peng, and M. Yang, Catal. Lett. **80**, 11 (2002).
[13] H. Sun, X. Pang, M. Chen, and Q. Shen, Catal. Lett. **90**, 85 (2003).
[14] Q. Shao, H. Sun, X. Pang, and Q. Shen, Eur. Polym. J. **40**, 97 (2004).
[15] X. Zhan, M. Yang, and H. Sun, Catal. Lett. **70**, 79 (2000).
[16] X. Zhan and M. Yang, J. Mol. Catal. A Chem. **169**, 27 (2001).
[17] M.A. Garcia and M.D. Morse, J. Phys. Chem. A **117**, 9860 (2013).
[18] D.J. Brugh and M.D. Morse, J. Chem. Phys. **141**, 064304/1 (2014).
[19] D.J. Brugh, R.S. DaBell, and M.D. Morse, J. Chem. Phys. **121**, 12379 (2004).
[20] T. Drewello and H. Schwarz, Chem. Phys. Lett. **171**, 5 (1990).
[21] J.M. Behm, C.A. Arrington, and M.D. Morse, J. Chem. Phys. **99**, 6409 (1993).
[22] J.C. Fabbi, L. Karlsson, J.D. Langenberg, Q.D. Costello, and M.D. Morse, J. Chem. Phys. **118**, 9247 (2003).
[23] Z. Fu and M.D. Morse, J. Chem. Phys. **90**, 3417 (1989).
[24] E.M. Spain and M.D. Morse, J. Chem. Phys. **97**, 4633 (1992).
[25] S.J. Dixon-Warren, R.F. Gunion, and W.C. Lineberger, J. Chem. Phys. **104**, 4902 (1996).
[26] G.K. Rothschopf and M.D. Morse, J. Phys. Chem. A **109**, 11358 (2005).
[27] J.A. Gray, S.F. Rice, and R.W. Field, J. Chem. Phys. **82**, 4717 (1985).
[28] J.A. Gray, R.W. Field, J. Chem. Phys. **84**, 1041 (1986).
[29] S. Adakkai Kadavathu, S. Loefgren, and R. Scullman, Phys. Scr. **35**, 277 (1987).
[30] S.A. Kadavathu, R. Scullman, J.A. Gray, M. Li, and R.W. Field, J. Mol. Spectrosc. **140**, 126 (1990).
[31] J.A. Gray, M. Li, and R.W. Field, J. Chem. Phys. **92**, 4651 (1990).
[32] J.A. Gray, M. Li, T. Nelis, and R.W. Field, J. Chem. Phys. **95**, 7164 (1991).
[33] S.A. Kadavathu, R. Scullman, R.W. Field, J.A. Gray, and M. Li, J. Mol. Spectrosc. **147**, 448 (1991).
[34] E.M. Spain and M.D. Morse, J. Chem. Phys. **97**, 4605 (1992).
[35] W.S. Tam, J.W.H. Leung, S.-M. Hu, and A.S.C. Cheung, J. Chem. Phys. **119**, 12245 (2003).
[36] W.S. Tam, J. Ye, and A.S.C. Cheung, J. Chem. Phys. **121**, 9430 (2004).
[37] T. Miyazawa, Y. Okabayashi Emi, F. Koto, M. Tanimoto, and T. Okabayashi, J. Chem. Phys. **124**, 224321 (2006).
[38] A.S.C. Cheung, H.F. Pang, W.S. Tam, and J.W.H. Leung, J. Chem. Phys. **131**, 194301/1 (2009).
[39] V.L. Ayles, L.G. Muzangwa, and S.A. Reid, Chem. Phys. Lett. **497**, 168 (2010).
[40] J.W.H. Leung, X. Wang, and A.S.C. Cheung, J. Chem. Phys. **117**, 3694 (2002).
[41] E. Yamazaki, T. Okabayashi, and M. Tanimoto, J. Chem. Phys. **121**, 162 (2004).
[42] J. Ye, J.W.H. Leung, and A.S.C. Cheung, J. Chem. Phys. **125**, 214308/1 (2006).
[43] L.G. Muzangwa, V.L. Ayles, S. Nyambo, and S.A. Reid, J. Mol. Spectrosc. **269**, 36 (2011).
[44] A.B. Darji and M.B. Sureshkumar, Indian J. Pure Appl. Phys. **28**, 338 (1990).
[45] T. Hirao, C. Dufour, B. Pinchemel, and P.F. Bernath, J. Mol. Spectrosc. **202**, 53 (2000).
[46] A. Poclet, Y. Krouti, T. Hirao, B. Pinchemel, and P.F. Bernath, J. Mol. Spectrosc. **204**, 125 (2000).
[47] Y. Krouti, A. Poclet, T. Hirao, B. Pinchemel, and P.F. Bernath, J. Mol. Spectrosc. **210**, 41 (2001).
[48] J.J. O'Brien, J.S. Miller, and L.C. O'Brien, J. Mol. Spectrosc. **211**, 248 (2002).
[49] L.C. O'Brien, K.M. Homann, T.L. Kellerman, and J.J. O'Brien, J. Mol. Spectrosc. **211**, 93 (2002).
[50] C.A. Rice and L.C. O'Brien, J. Mol. Spectrosc. **221**, 131 (2003).
[51] S. Tumturk, L.C. O'Brien, and J.J. O'Brien, J. Mol. Spectrosc. **225**, 225 (2004).
[52] C.A. Rice, T.L. Kellerman, B. Owen, L.C. O'Brien, H. Cao, and J.J. O'Brien, J. Mol. Spectrosc. **235**, 271 (2006).
[53] B. Pinchemel, Y. Lefebvre, and J. Schamps, J. Mol. Spectrosc. **77**, 29 (1979).
[54] R. Gopal and M.M. Joshi, Curr. Sci. **50**, 530 (1981).
[55] J. Bai and R.C. Hilborn, Chem. Phys. Lett. **128**, 133 (1986).
[56] A. Bouddou, C. Dufour, and B. Pinchemel, J. Mol. Spectrosc. **168**, 477 (1994).
[57] C. Dufour, I. Hikmet, and B. Pinchemel, J. Mol. Spectrosc. **165**, 398 (1994).

[58] C. Dufour and B. Pinchemel, J. Mol. Spectrosc. **173**, 70 (1995).
[59] C. Focsa, C. Dufour, and B. Pinchemel, J. Mol. Spectrosc. **182**, 65 (1997).
[60] Y. Chen, J. Jin, C. Hu, X. Yang, X. Ma, and C. Chen, J. Mol. Spectrosc. **203**, 37 (2000).
[61] J. Jin, Y. Chen, X. Yang, Q. Ran, and C. Chen, J. Mol. Spectrosc. **208**, 18 (2001).
[62] J. Jin, Q. Ran, X. Yang, Y. Chen, and C. Chen, J. Phys. Chem. A **105**, 11177 (2001).
[63] M. Tanimoto, T. Sakamaki, and T. Okabayashi, J. Mol. Spectrosc. **207**, 66 (2001).
[64] Y. Krouti, T. Hirao, C. Dufour, A. Boulezhar, B. Pinchemel, and P.F. Bernath, J. Mol. Spectrosc. **214**, 152 (2002).
[65] B. Pinchemel, T. Hirao, and P.F. Bernath, J. Mol. Spectrosc. **215**, 262 (2002).
[66] M. Benomier, A. Van Groenendael, B. Pinchemel, T. Hirao, and P.F. Bernath, J. Mol. Spectrosc. **233**, 244 (2005).
[67] R.A. Harris, L.C. O'Brien, and J.J. O'Brien, J. Mol. Spectrosc. **259**, 116 (2010).
[68] C.T. Kingston, A.J. Merer, and T.D. Varberg, J. Mol. Spectrosc. **215**, 106 (2002).
[69] P.M. Sheridan and L.M. Ziurys, J. Chem. Phys. **118**, 6370 (2003).
[70] A.L. Allred, J. Inorg. Nucl. Chem. **17**, 215 (1961).
[71] M.D. Moran, J.-P. Jones, A.A. Wilson, S. Houle, G.K. Surya Prakash, G.A. Olah, and N. Vasdev, Chem. Educ. **16**, 164 (2011).
[72] E.M. Spain and M.D. Morse, J. Chem. Phys. **97**, 4641 (1992).
[73] P. Carette, C. Dufour, andB. Pinchemel, J. Mol. Spectrosc. **161**, 323 (1993).
[74] J.T. Hougen, J. Mol. Spectrosc. **267**, 23 (2011).
[75] L. Shao, S.M. Sickafoose, J.D. Langenberg, D.J. Brugh, and M.D. Morse, J. Chem. Phys. **112**, 4118 (2000).
[76] N. Lindholm and M.D. Morse, J. Chem. Phys. **127**, 084317/1 (2007).
[77] A. Martinez, N. Lindholm, and M.D. Morse, J. Chem. Phys. **135**, 134308/1 (2011).
[78] W.C. Wiley and I.H. McLaren, Rev. Sci. Instrum. **26**, 1150 (1955).
[79] B.A. Mamyrin, V.I. Karataev, D.V. Shmikk, and V.A. Zagulin, Zh. Eksp. Teor. Fiz. **64**, 82 (1973).
[80] S. Gerstenkorn and P. Luc, *Atlas du Spectre d'Absorption de la Molécule d'Iode entre 14,800–20,000 cm^{-1}* (CNRS, Paris, 1978).
[81] S. Gerstenkorn and P. Luc, Rev. Phys. Appl. **14**, 791 (1979).
[82] M.D. Morse, in *Methods of Experimental Physics: Atomic, Molecular, and Optical Physics*, edited by F.B. Dunning and R. Hulet (Academic Press Inc., Orlando, FL, 1996), p. 21.
[83] P.R. Bevington, *Data Reduction and Error Analysis for the Physical Sciences* (McGraw-Hill, New York, 1969).
[84] T.H. Dunning, Jr., J. Chem. Phys. **90**, 1007 (1989).
[85] M.J. Frisch, G.W. Trucks, H.B. Schlegel, G.E. Scuseria, M.A. Robb, J.R. Cheeseman, G. Scalmani, V. Barone, B. Mennucci, G.A. Petersson, H. Nakatsuji, M. Caricato, X. Li, H.P. Hratchian, A.F. Izmaylov, J. Bloino, G. Zheng, J.L. Sonnenberg, M. Hada, M. Ehara, K. Toyota, R. Fukuda, J. Hasegawa, M. Ishida, T. Nakajima, Y. Honda, O. Kitao, H. Nakai, T. Vreven, J.A. Montgomery, Jr., J.E. Peralta, F. Ogliaro, M. Bearpark, J.J. Heyd, E. Brothers, K.N. Kudin, V.N. Staroverov, R. Kobayashi, J. Normand, K. Raghavachari, A. Rendell, J.C. Burant, S.S. Iyengar, J. Tomasi, M. Cossi, N. Rega, J.M. Millam, M. Klene, J.E. Knox, J.B. Cross, V. Bakken, C. Adamo, J. Jaramillo, R. Gomperts, R.E. Stratmann, O. Yazyev, A.J. Austin, R. Cammi, C. Pomelli, J.W. Ochterski, R.L. Martin, K. Morokuma, V.G. Zakrzewski, G.A. Voth, P. Salvador, J.J. Dannenberg, S. Dapprich, A.D. Daniels, Ö. Farkas, J.B. Foresman, J.V. Ortiz, J. Cioslowski, and D.J. Fox, Gaussian 09, Revision D.01 (Gaussian Inc., Wallingford CT, 2009).
[86] H. Lefebvre-Brion and R.W. Field, *The Spectra and Dynamics of Diatomic Molecules* (Elsevier, Amsterdam, 2004).
[87] G. Herzberg, *Molecular Spectra and Molecular Structure I. Spectra of Diatomic Molecules* (Van Nostrand Reinhold, New York, 1950).
[88] PGOPHER. *A Program for Simulating Rotational Structure*, *C.M. Western, University of Bristol*. http://pgopher.chm.bris.ac.uk
[89] T.G. Dietz, M.A. Duncan, A.C. Puiu, and R.E. Smalley, J. Phys. Chem. **86**, 4026 (1982).
[90] T.G. Dietz, M.A. Duncan, and R.E. Smalley, J. Chem. Phys. **76**, 1227 (1982).
[91] N.F. Lindholm, D.J. Brugh, G.K. Rothschopf, S.M. Sickafoose, and M.D. Morse, J. Chem. Phys. **118**, 2190 (2003).
[92] D.J. Brugh and M.D. Morse, J. Chem. Phys. **117**, 10703 (2002).
[93] M.D. Morse, G.P. Hansen, P.R.R. Langridge-Smith, L.-S. Zheng, M.E. Geusic, D.L. Michalopoulos, and R.E. Smalley, J. Chem. Phys. **80**, 5400 (1984).
[94] J.C. Pinegar, J.D. Langenberg, C.A. Arrington, E.M. Spain, and M.D. Morse, J. Chem. Phys. **102**, 666 (1995).
[95] S. Taylor, E.M. Spain, and M.D. Morse, J. Chem. Phys. **92**, 2710 (1990).
[96] S. Taylor, E.M. Spain, and M.D. Morse, J. Chem. Phys. **92**, 2698 (1990).

Downloaded by [University of Utah] at 12:10 13 September 2015